www.springer.com/41230
https://doi.org/10.1007/s41230-024-2147-5

Synergistic effect of Zr and Mo on precipitation and high-temperature properties of Al-Si-Cu-Mg alloys

Chao Gao[1], *Bing-rong Zhang[1], Yin-ming Li[2], Zhi-ming Wang[1], and Xiang-bin Meng[1]

1. Faculty of Mechanical Engineering, Qilu University of Technology (Shandong Academy of Sciences), Jinan 250353, China

2. Hebei Ounai Machinery Mould Co. Ltd., Xingtai 054500, Hebei, China

Abstract: This study focuses on finding a solution to the sharp decline in mechanical properties of Al-Si-Cu-Mg alloys due to rapid coarsening of traditional intermediate phases at high temperature. A new type of modified alloy, to be used in automobile engines at high temperatures, was prepared by adding Zr and Mo into Al-Si-Cu-Mg alloy. The synergistic effects of Zr and Mo on the microstructure evolution and high-temperature mechanical properties were studied. Results show that the addition of Zr and Mo generates a series of intermetallic phases dispersed in the alloy. They can improve the strength of the alloy by hindering dislocation movement and crack propagation. In addition, some nano-strengthened phases show coherent interfaces with the matrix and improve grain refinement. The addition of Mo greatly improves the heat resistance of the alloy. The extremely low diffusivity of Mo enables it to improve the thermal stability of the intermetallic phases, inhibit precipitation during aging, reduce the size of the precipitates, and improve the heat resistance of the alloy.

Keywords: Al-Si-Cu-Mg alloy; high-temperature properties; Zr-Mo-rich intermetallics; nano-strengthening phases

CLC numbers: TG146.21 **Document code:** A **Article ID:** 1672-6421(2024)01-071-11

1 Introduction

With the development of future automobile engines directed toward contradictory goals of high load stress and thin-walled structures, more demanding requirements are put forward for the materials used in their manufacture. This trend is bound to result in higher working temperatures over 250 °C in engines, and thus, higher detonation pressures during operation. As lightweight materials with excellent casting properties and good overall performance, Al-Si casting alloys have been widely used in the manufacture of premium passenger car engines [1]. Al-Si alloys are strengthened by traditional intermediate phases such as Al_2Cu, Q-$Al_5Mg_8Si_4Cu_2$ and Mg_2Si dispersed in the matrix. However, these traditional intermediate phases rapidly coarsen and lose their strengthening effect at approximately 200 °C, resulting in a sharp decline in the mechanical properties of Al-Si casting alloys, which severely limits their applications [2-5]. Optimization of the high-temperature mechanical properties of Al-Si casting alloys, especially when the working temperature is above 200 °C, has received much attention from researchers around the world.

Studies on optimizing high-temperature mechanical properties of Al-Si casting alloys focus on several approaches. One method is to strengthen aluminum alloys through preparation of composite materials, but the preparation process is generally complicated, and the manufacturing cost is high [6, 7]. Another approach is the optimization of the heat treatment process. Although the optimization of the heat treatment process can greatly improve the mechanical properties of Al-Si casting alloys at room temperature, the high-temperature mechanical properties are low due to coarsening of intermediate phase [8-11]. The most commonly used method to improve the high-temperature mechanical properties of the alloy is microalloying. The microalloying elements react with the base alloy and form heat-resistant intermediate phases that stabilize and strengthen the base alloy at temperatures where traditional hardening phases no longer work [12, 13].

***Bing-rong Zhang**

Male, born in 1958, Ph.D, Professor. Research interest: Nonferrous alloys applications in automobiles and aircraft.

E-mail: brzit@aliyun.com

Received: 2022-12-28; Accepted: 2023-11-11

The strengthening effect of microalloying is extremely dependent on the morphology, particle size and distribution of the thermally stable intermediate phases. Hernandez-Sandoval et al. [14, 15] found that when Ni was added to an Al-Si casting alloy, Cu atoms preferentially combined with Ni to form a large-sized Al_3CuNi phase that reduced the strength of the alloy to a certain extent. The generated acicular Al_9NiFe phase significantly reduced the toughness of the alloy. According to many research results, heat-resistant intermetallic phases rich in transition metal elements tend to be larger in size [2, 16-18] because they have higher melting points, and often form during the solidification stage. Although these large intermediate phases enhance the high-temperature properties of the alloys, they easily become sites where cracks initiate during fracture, which have a certain negative impact on the mechanical properties of the alloys. Phases with dispersed small particles are a better choice for strengthening alloys. Many studies have shown that some transition metal elements combined with Al to form thermally stable Al_3M-trialuminides [19-22]. The high-symmetry cubic $L1_2$ and related tetragonal $D0_{22}$ and $D0_{23}$ structures are prevalent among transition elements. Many studies have shown that Al_3M-trialuminides can be easily formed by adding Zr and Sc [23-26]. As a rare earth element, Sc has a good enhancement effect on high-temperature performance of aluminum alloys, but it is expensive and difficult to use widely in actual production. Zr expands slowly in α-Al, but the $L1_2$ structure of Al_3Zr is thermodynamically metastable. The precipitates are kinetically stable below 475 °C, while Al_3Zr precipitates with $L1_2$ structure coarsen and transform into the equilibrium $D0_{23}$ structure at higher temperatures [27]. In addition, some researchers have reported the effect of Zr on grain refinement. Liu et al. [28] mentioned that the addition of 0.1wt.% Zr had no significant effect on grain size of Al-7Si-0.45Mg, but when the addition of Zr exceeded its maximum solubility (0.11%), the continued addition of Zr significantly reduced the grain size. When the Zr content was 0.2wt.%, the grain size decreased sharply, but if the Zr content further continued to increase, the rate of grain refinement slowed.

Some research shows molybdenum (Mo) can participate in the synthesis of various intermetallic phases enriched with other transition metal elements [29]. Molybdenum has very low diffusivity and solid solubility in Al at high temperature, which is of great benefit for thermally stable phases that resist coarsening. Meanwhile, the low diffusivity of Mo and delaying precipitation during aging are expected to prevent the formation of large intermetallic phases. Farkoosh et al. [30] found that adding 0.3wt.% Mo to Al-7Si-Cu-Mg could increase the ultimate tensile strength by 15% and yield strength by 25% at 300 °C. Furthermore, Zamani et al. [31] added Mo to $AlSi_{10}Cu_3Mg$, and found that the room temperature tensile strength and elongation were both affected by the Mo content. When the content of Mo exceeded 0.25%, the maximum solubility of Mo in Al, coarse and irregularly shaped Mo-rich phases were generated in the matrix, which had an extremely negative effect on the tensile behavior of the alloy. To date, there are still few studies on the influence of Mo addition on the structure and morphology of intermetallic phases formed in Al-Si alloys at high temperature, and further exploration will be of great help to the development of new heat-resistant aluminum alloys.

Considering the slow diffusion of Mo and its ability to participate in the formation of a variety of intermediate phases that inhibit precipitation as well as the excellent strengthening effect of the Al_3Zr-type phase, the synergistic effects of Mo and Zr addition on the formation and particle size of the intermetallic phases in Al-Si-Cu-Mg alloy were investigated in this study. The strengthening effect was verified by high-temperature mechanical property testing, and the high-temperature strengthening mechanism was explored in combination with the microstructural changes caused by the synergistic effects of Zr and Mo.

2 Experimental

2.1 Preparation of test bar

The experimental alloys were prepared in an induction furnace (GR3-100-9, Huazong Furnaces Co., Ltd., Dongguan, China) by the addition of commercial alloys of Al-40Cu, Al-30Si, Al-10Ti, Al-10Zr, and Al-5Mo and pure Al and Mg to obtain the desired alloy. A spectrometer (S600, Boyue Instruments Co., Ltd., Nanjing, China) was used to detect the chemical composition of the prepared alloys, and the results are shown in Table 1. Refiner Al-5Ti-1B and modifier Al-10Sr were added after alloy completely melted. After adding the refiner and modifier and continuing to hold for 15 min at 800 °C, the alloy was poured into a permanent mold at 740 °C. In a similar way, the Al-Si-Cu-Mg base alloy was also cast in a permanent mold.

After casting, the Al-Si-Cu-Mg and Al-Si-Cu-Mg-(Zr-Mo) alloys were subjected to heat treatment using a high temperature muffle furnace (SX2-8-16T, Shanghai Hengyue Medical Equipment Co., Ltd., Shanghai, China), which has a temperature controlled accuracy within ±5 °C. Solution treatments at different temperatures were performed on the two alloys, and the corresponding solution parameters are shown in Table 2. Then, all alloys were quenched in water at 60 °C, then

Table 1: Chemical composition of Al-Si-Cu-Mg with and without addition of transition metal elements (wt.%)

Alloy	Si	Cu	Mg	Fe	Sr	Ti	Zr	Mo	Al
Al-Si-Cu-Mg	9.0	1.0	0.36	0.15	0.005	0.13	–	–	Bal.
Al-Si-Cu-Mg-(Zr-Mo)	9.1	1.0	0.35	0.14	0.005	0.13	0.22	0.21	Bal.

aged at 100 °C for 3 h and aged at 180 °C for 9 h, then cooled to room temperature in the furnace. (Unless specifically noted, the solution treatment parameters used for the modified alloy were 500 °C for 4 h and 550 °C for 5 h). All castings were processed and machined according to GB/T 6397-86.

Table 2: Solid solution process parameters

Alloy	Solid solution process parameters
Al-Si-Cu-Mg	500 °C for 4 h and 520 °C for 5 h
Al-Si-Cu-Mg-(Zr-Mo)	500 °C for 4 h and 520 °C for 5 h
	500 °C for 4 h and 530 °C for 5 h
	500 °C for 4 h and 540 °C for 5 h
	500 °C for 4 h and 550 °C for 5 h
	500 °C for 4 h and 560 °C for 5 h

2.2 Microscopic morphology observation and mechanical property testing

Specimens for microstructural characterization were prepared using a standard metallographic technique, and polished to mirror-like surfaces using alumina particles. Specimens were etched using Keler reagent (2.5% HNO_3+1.5% HCl+1% HF +95% H_2O) to reveal the intermetallic morphology. The microscopic morphology of the heat-treated specimens was observed by optical microscopy (OM, Leica DM2700 M) equipped with an ISA4 metallographic image quantitative analysis system, scanning electron microscopy (SEM, Zeiss SU-PRA55) equipped with an energy disperse system (EDS), and transmission electron microscopy (TEM, FEI Talos F200X) equipped with an EDS. Phase transformation analysis was conducted by differential scanning calorimetry (DSC), using Netzsch DSC404 F3 equipment. The spacing between multiple dendrites at different positions can be measured by ISA4 system. The measurement value can be divided by the number of dendrites to obtain the secondary dendrite arm spacing at that location. By averaging the different secondary dendrite arm spacing at multiple positions, the average secondary dendrite arm spacing (SDAS) of the alloy can be obtained. The processed test bar was subjected to tensile testing on an electronic universal testing machine (DDL100, Changchun Institute of Mechanical Science Co., Ltd.) with test temperatures of 25, 80, 160, 240, and 300 °C at a strain rate of 2 mm·min^{-1}. Shape and size of tensile specimen are shown in Fig. 1. Before the tensile test, the tensile specimens were heated to the test temperature in a chamber at a rate of 10 °C·min^{-1} and kept for 20 min.

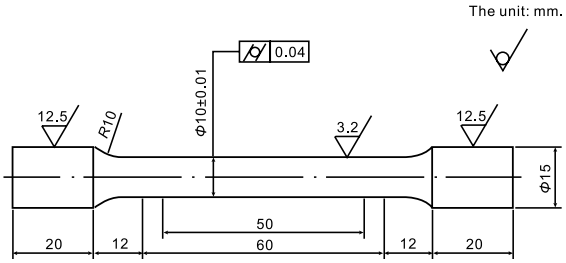

Fig. 1: Shape and size of tensile specimen

3 Results

3.1 Microstructural analysis

The microstructures of Al-Si-Cu-Mg and Al-Si-Cu-Mg-(Zr-Mo) alloys after T6 heat treatment are shown in Fig. 2. EDS analysis was performed for the intermetallic phase, and the corresponding results are shown in Table 3. The analysis results are combined with Refs. [16, 17, 32].

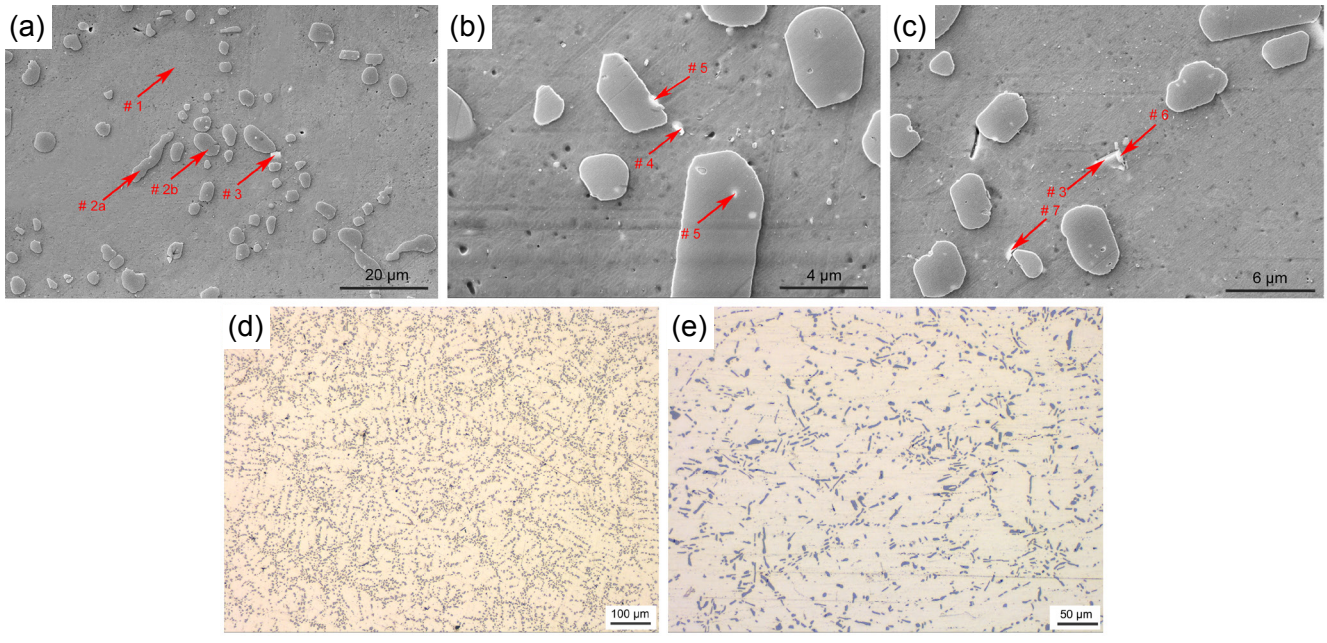

Fig. 2: Microstructure of Al-Si-Cu-Mg alloy with (a, b, c, d) and without (e) transition metal elements Zr and Mo after T6 heat treatment

Table 3: Main phases and their morphologies identified using SEM/EDS in Al-Si-Cu-Mg alloy modified with Zr and Mo and in Refs. [16, 17, 32, 33]

No.	Phases calculated from components identified by EDS	Phases from Refs. [16, 17, 32, 33]	Phase morphology
#1	α-Al	α-Al	Dendritic
#2a	Eutectic Si	Eutectic Si	Fibrous like
#2b	Eutectic Si	Eutectic Si	Granular
#3	$Al_5Si_{1.8}TiZr_{2.1}$	$(AlSi)_3(TiZr)$	Blocky
#4	$Al_9Si_{2.9}Cu_{1.2}Mo_{0.4}$	$Al\text{-}Al_2Cu\text{-}Si$	Blocky
#5	$Al_{56}Si_{38}Fe_3Mo_{1.2}$	AlSiFeMo	Granular
#6	$Al_{5.1}Si_{32}Ti_{0.5}Zr_{2.1}Fe_{0.7}$	$(AlSi)_2(TiZr)Fe$	Needle-like
#7	$Al_{4.8}Si_{2.2}Zr_{2.1}$	$(AlSi)_3Zr$	Pipe-like

After adding the transition metal elements Zr and Mo to Al-Si-Cu-Mg, four new intermetallic phases are formed: blocky $(AlSi)_3(TiZr)$ (#3), granular AlSiFeMo (#5), needle-like $(AlSi)_2(TiZr)Fe$ (#6), and pipe-like $(AlSi)_3Zr$ (#7) [16, 17, 32, 33]. There are two different morphologies of eutectic silicon, fibrous and granular. In Al-Si-Cu-Mg-(Zr-Mo) alloy, the eutectic silicon is mainly granular, and a very small proportion of fibrous eutectic silicon exists. Notably, the intermetallic phase in Al-Si-Cu-Mg-(Zr-Mo) is smaller in size, which is beneficial for the improvement of the mechanical properties. The average measured size of the secondary dendrite arm spacing (SDAS) of the Al-Si-Cu-Mg-(Zr-Mo) after T6 is 14.85±0.21 μm, while that of the Al-Si-Cu-Mg is 23.65±0.57 μm, which is much larger than that of the Al-Si-Cu-Mg-(Zr-Mo).

Figure 3 shows the microstructure of the Al-Si-Cu-Mg-(Zr-Mo) after T6 heat treatment observed by TEM. The nano-intermetallic

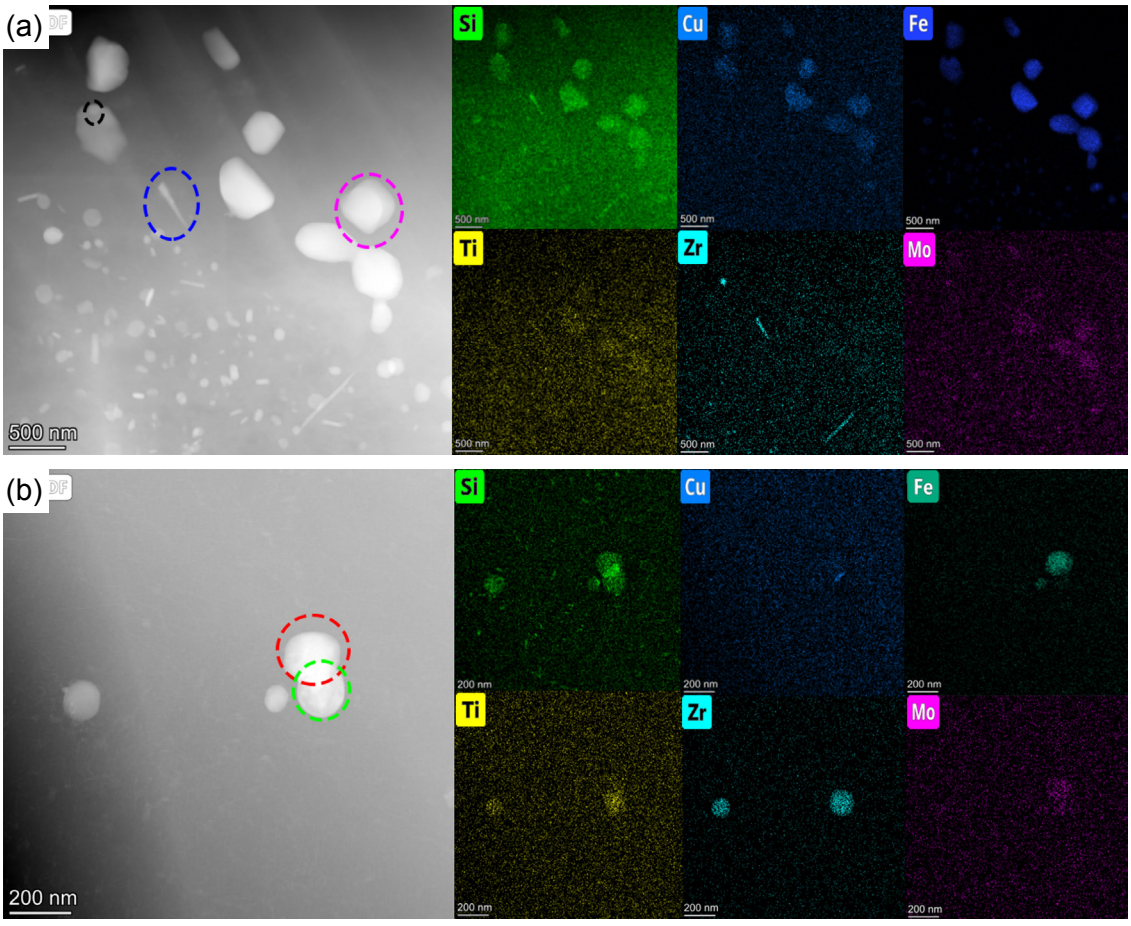

Fig. 3: TEM observations of nano-intermetallic phases in Al-Si-Cu-Mg-(Zr-Mo) after T6 heat treatment and corresponding EDS analysis

phase is dispersed with a particle size of 60–80 nm. Some larger particles with a size of 300–500 nm are also observed. The compositions contained in the intermetallic phase were identified by EDS, including AlSiCuFeMo (purple circus) and AlSiFeMo (red circus), granular AlSiZrMo (black circus) and $(Al,Si)_3(TiZr)$ (green circus), and needle-like $(Al,Si)_3Zr$ (blue circus). Some research works have found that the addition of Zr led to the formation of the nano-strengthened phase Al_3Zr in the alloy [21, 25, 26], however, Al_3Zr is not observed in this research.

The microstructures of the Al-Si-Cu-Mg-(Zr-Mo) under different solid solution processes are shown in Fig. 4. In our previous study, the peak mechanical properties of Al-Si-Cu-Mg were observed for a second-stage solution temperature of 520 °C [32]. However, when Al-Si-Cu-Mg-(Zr-Mo) was heat-treated at the same temperature, obvious agglomeration of the eutectic silicon is observed [Fig. 4(a)]. When the second-stage solution temperature is further increased to 530 °C, a large amount of agglomeration of eutectic silicon still exists [Fig. 4(b)]. It is reasonable to speculate that the second-stage solution temperature of 520 °C is insufficient to obtain a homogenized structure for Al-Si-Cu-Mg-(Zr-Mo). Therefore, Al-Si-Cu-Mg-(Zr-Mo) was heat treated at a higher second-stage solution temperature. In Fig. 4(c), corresponding to the second-stage solution temperature of 550 °C, the eutectic silicon is uniformly distributed, and the morphology is granular, fiber-like, almost invisible. In Fig. 4(d), there are many traces of liquid flow left by overburning (red arrows) when the solution temperature reaches 560 °C.

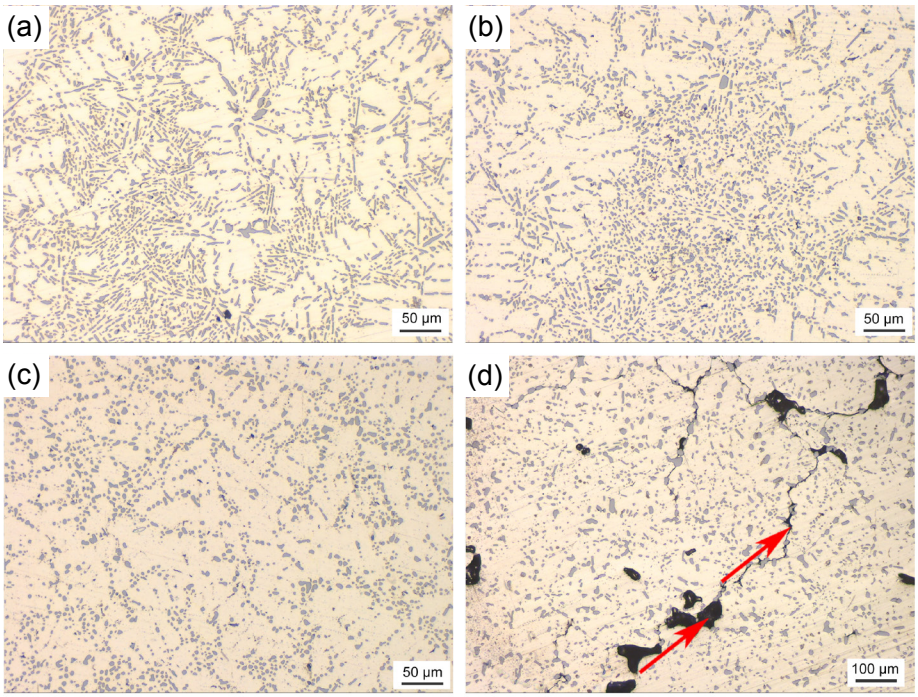

Fig. 4: OM microstructures of Al-Si-Cu-Mg-(Zr-Mo) during T6 heat treatment (different second-stage solution temperatures): (a) 520 °C; (b) 530 °C; (c) 550 °C; (d) 560 °C

3.2 Tensile properties

Tensile tests were performed at room temperature to test the influence of the second-stage solution temperature on the mechanical properties, and the test results are shown in Fig. 5. When the second-stage solution temperature reaches 560 °C, the Al-Si-Cu-Mg-(Zr-Mo) is overburned, and it is no longer suitable for experimental measurements of mechanical properties. The peak mechanical properties of Al-Si-Cu-Mg-(Zr-Mo) are observed when the second-stage solution temperature is 550 °C.

The ultimate tensile strength (UTS), yield strength (YS) and elongation of the Al-Si-Cu-Mg-(Zr-Mo) and the Al-Si-Cu-Mg after T6 treatment tested at different temperatures are plotted in Fig. 6. The UTS and YS of the Al-Si-Cu-Mg-(Zr-Mo) alloy after the T6 heat treatment are greater than those of Al-Si-Cu-Mg at all test temperatures (25–300 °C), and a superior strengthening effect is displayed with increasing test temperature. When the test temperature is 25 °C, the UTS of Al-Si-Cu-Mg-(Zr-Mo) and Al-Si-Cu-Mg is almost the same,

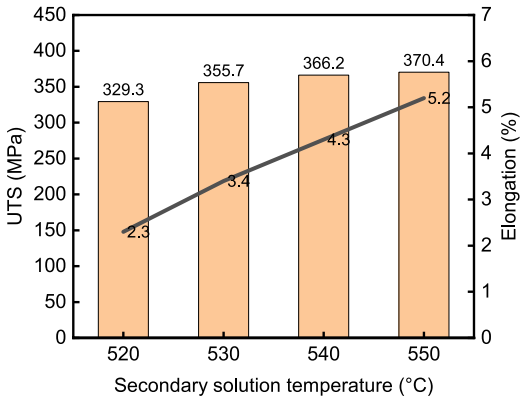

Fig. 5: Effects of different second-stage solution temperatures on mechanical properties of Al-Si-Cu-Mg-(Zr-Mo)

370.4 MPa and 369.1 MPa, respectively. When the test temperature is raised to 300 °C, the UTS of Al-Si-Cu-Mg-(Zr-Mo) and Al-Si-Cu-Mg is 173.6 MPa and 93.7 MPa, respectively. At this test temperature, the addition of Zr and Mo increases the UTS of the alloy by 85%. However, the elongation of the modified alloy displays the opposite trend, i.e., it is lower than that of Al-Si-Cu-Mg at all test temperatures.

The mechanical property changes of Al-Si-Cu-Mg-(Zr-Mo) with increasing temperature show a more sensitive trend at 160 °C. When the test temperature is lower than 160 °C, the UTS, YS, and percentage elongation of Al-Si-Cu-Mg, compared with Al-Si-Cu-Mg-(Zr-Mo), are decreased by 62.4 MPa, 45.6 MPa, and −2.08%, respectively, for every 80 °C increase in test temperature. While, as the test temperature is higher than 160 °C, the UTS, YS, and elongation of Al-Si-Cu-Mg are decreased by 96.8 MPa, 89.6 MPa, and −4.64%, respectively for every 80 °C increase in test temperature than Al-Si-Cu-Mg-(Zr-Mo). However, in test temperature range of 25–300 °C, the mechanical properties of Al-Si-Cu-Mg-(Zr-Mo) almost always show a linear relationship with the test temperature.

3.3 Characterization of tensile fracture

Figure 7 shows the fracture surfaces of Al-Si-Cu-Mg-(Zr-Mo) after T6 treatment at different tensile testing temperatures of 25 °C, 80 °C, 160 °C, 240 °C, and 300 °C. Generally, brittle fracture is due to the strong interaction between plastic flow or dislocation slip bands and the precipitation of the dispersed phase, especially at the grain boundaries, resulting in the spalling of some precipitates from the matrix, accompanied by the extension and connection of microcracks [16], usually manifested as microcracks (indicated by red arrows). On the tensile fracture surfaces corresponding to room temperature and 80 °C [Figs. 7(a, b)], more microcracks are accompanied by tear ridge features, and some small areas show a high density of secondary cracks (white dotted circles). When the test temperature is raised to 160 °C, although there are still many microcracks [Fig. 7(c)], some features similar to dimples appear, and the tensile fracture behavior of the specimen corresponding to this sample should still be defined as brittle fracture. As the test temperature increases, the characteristics of ductile fractures appear and become obvious, and the characteristics of brittle fractures decrease, even disappear. Figure 7(d) shows the fracture surface of the specimen after tensile testing at 240 °C. A more typical ductile fracture feature (dimple feature) appears (marked by blue arrows). The ductile

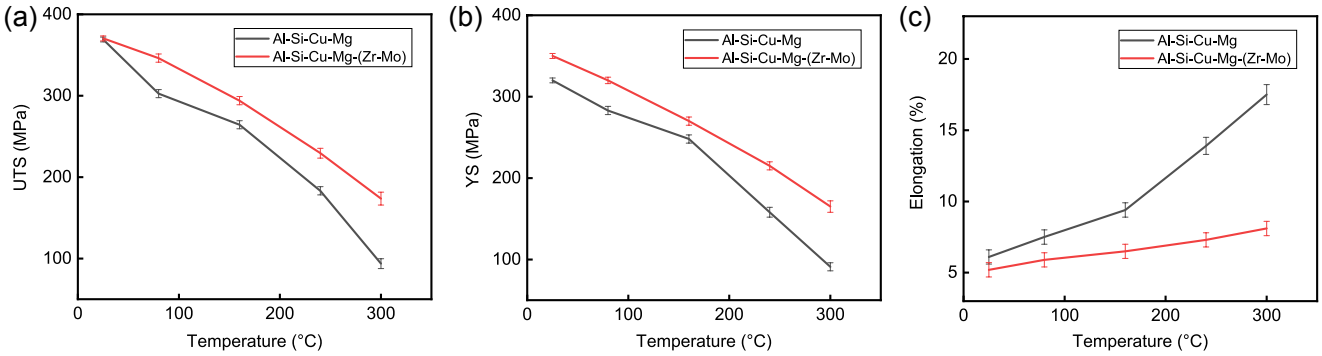

Fig. 6: Comparison of tensile properties of Al-Si-Cu-Mg-(Zr-Mo) with Al-Si-Cu-Mg in T6 heat-treated condition obtained at different testing temperatures: (a) ultimate tensile strength; (b) yield strength; (c) elongation

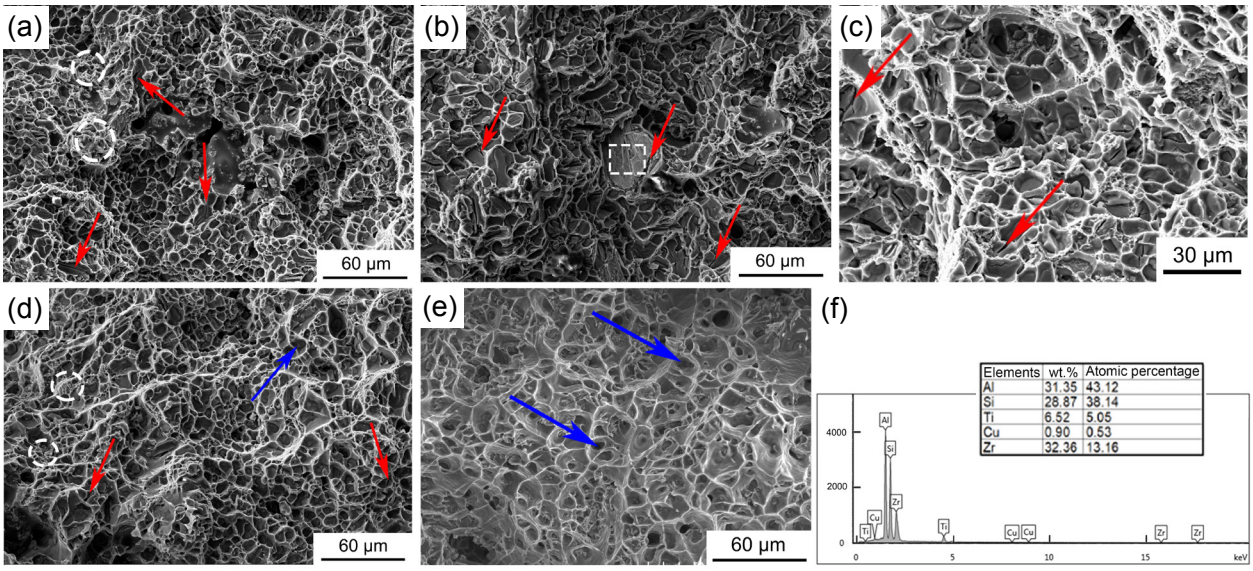

Fig. 7: Tensile fracture morphologies of Al-Si-Cu-Mg-(Zr-Mo) after T6 treatment at different test temperatures: (a) 25 °C; (b) 80 °C; (c) 160 °C; (d) 240 °C; (e) 300 °C; (f) EDS analysis of the area enclosed by the white dashed box in Fig. 7(b)

fracture features in a larger area are still mixed with some microcracks, and high-density secondary cracks are present in a small area. At this time, the fracture mode of the alloy changes from brittle fracture to mixed fracture. Figure 7(e) shows the fully ductile fracture characteristics, which mean that the tensile fracture of the alloy transforms into a fully ductile fracture at tensile testing temperature of 300 °C.

Figure 7(f) shows the result of the EDS analysis of the area enclosed by the white dashed box in Fig. 7(b), which is determined to be the $(Al,Si)_3(TiZr)$ phase and verified by Ref. [16]. However, such a large $(Al,Si)_3(TiZr)$ particle is seldom found during the metallographic observations discussed in Section 3.1.

4 Discussion

As noted in Section 3.2, Al-Si-Cu-Mg-(Zr-Mo) shows great advantages over Al-Si-Cu-Mg in terms of mechanical properties. Improvements in alloy properties are usually caused by modification of their microstructure. It is clear that Al-Si-Cu-Mg-(Zr-Mo) shows smaller SDAS, thus the higher YS of Al-Si-Cu-Mg-(Zr-Mo) at room temperature can be explained. In general, a smaller SDAS means more grain boundaries present in the alloy, greater resistance to dislocation movement, and better YS of the alloy [34]. The intermetallic phases rich in transition metal elements with good thermal stability have a positive effect on the strength properties of the alloy while a slight negative effect on the elongation, which results in the smaller elongation of Al-Si-Cu-Mg-(Zr-Mo) at all test temperatures. These heat-resistant intermetallic phases continue to enhance the strengthening effect of the alloy after the traditional intermetallic phases fails. At room temperature, due to the presence of many traditional strengthening phases such as θ-Al_2Cu, Q-$Al_5Mg_8Si_4Cu_2$, intermetallic phases enriched with transition metal elements have little effect on enhancement of the strength properties of the alloy. However, with increasing test temperature, the positive contributions of the intermetallic phases enriched in transition metal elements to the strength properties of the alloy become obvious, especially at the coarsening temperature of traditional intermetallic phases.

This is consistent with the fact that the strength of Al-Si-Cu-Mg-(Zr-Mo) decreases more slowly than that of Al-Si-Cu-Mg as the test temperature increases above 160 °C. [Figs. 6(a) and (b)]. Among the intermetallic phases used for strengthening, small and dispersed intermetallic phases have better strengthening ability. Liu et al. [35-37] mentioned that the presence of nanoparticles could refine grains for most aluminum alloys. Mahmudi [38] claimed that Al_3Zr had a refining effect on grains. However, the Al_3Zr phase is not found in the present study, but the corresponding $(Al,Si)_3Zr$ phase is found. Gao et al. [39] noted that $(Al,Si)_3Zr$ may be caused by the high content of Si (9wt.%) in the alloy. Additionally, because Si and Al have similar structures, Si atoms can be replaced by Al atoms in the lattice to a certain extent. This change causes the intermetallic phase size to increase from 20 nm for Al_3Zr to 100 nm for $(Al,Si)_3Zr$ [39]. The size of $(Al,Si)_3Zr$ in this alloy is slightly smaller, approximately 60–80 nm, which is related to the difference in alloy material composition and casting process parameters, but it is basically consistent with the research results of Gao et al [39]. The $(Al,Si)_3(TiZr)$ phase is highly similar to the $(Al,Si)_3Zr$ phase in both size and morphology. Some Zr atoms in the original $(Al,Si)_3Zr$ phase are replaced by Ti atoms (introduced by grain refiners added to the alloy), which occupies the Zr position in the ordered Al_3Zr phase in $L1_2$ and participates in the formation of the Al-Si-Zr phase, thus generating $(Al,Si)_3(Ti_x,Zr_{1-x})$, which is consistent with the findings of Knipling et al [40, 41]. According to heterogeneous nucleation theory, the grain size is controlled by two factors: undercooling and nucleation sites. The addition of Zr and Mo to the alloy results in the formation of intermetallic compounds of Zr and Mo, which are stable at temperatures above 650 °C and can act as nucleation sites [25]. The Zr-containing phase is small in size and dispersed in a dense distribution, and the distance between the two phases is small. As the nucleation sites, the grown dendrites meet sooner and stop growing, which plays the role in grain refinement. The diffraction spots at the intersection of the AlSiFeMo phase and the matrix [red circled area in Fig. 8(a)] were imaged using TEM, and the results are shown in Fig. 8(c), where the diffraction spots of the α-Al matrix and the AlSiFeMo phase are both presented. The green circle shows where the diffraction spots overlap. The diffraction spots of the two objects do not completely overlap, indicating that the lattice still has a small degree of mismatch. The diffraction spots of the α-Al matrix and the AlSiFeMo phase are considered to be coincident. Thus, the α-Al matrix and the AlSiFeMo phase present a semicoherent interface. The intermetallic phase inside the green circle in Fig. 8(b) is determined to be the $(Al,Si)_3Zr$ phase after EDS scanning analysis and lattice diffraction spot calibration [Fig. 8(d)]. To explore the interface relationship, the interface junction between the $(Al,Si)_3Zr$ phase and the α-Al matrix (green circle) was photographed in high resolution mode, and Fig. 8(e) was obtained. The fast Fourier transformation of this image was calculated, as shown in Fig. 8(f). The calibration of the diffraction spots in Fig. 8(f) shows that the α-Al matrix and the $(Al,Si)_3Zr$ phase are completely coherent, and the mismatch between them is almost zero. The direct minimal mismatch between the two phases makes them effective as nucleation sites, which greatly improves the efficiency of grain refinement [42].

In Al-Si-Cu-Mg alloys, the mechanical properties are mainly provided by traditional intermetallic phases Al_2Cu, Q-$Al_5Cu_2Mg_8Si_6$, and some Fe-rich phases. The melting point of the Al_2Cu phase is 523 °C, and the melting point of the Q-$Al_5Cu_2Mg_8Si_6$ phase is 533 °C. When the alloy is kept at a higher temperature for a long time, these intermetallic phases coarsen and dissolve [3, 43, 44]. When Mo participates in the synthesis of other intermetallic phases, the thermal stability of intermetallic phases can be improved due to the slow diffusion

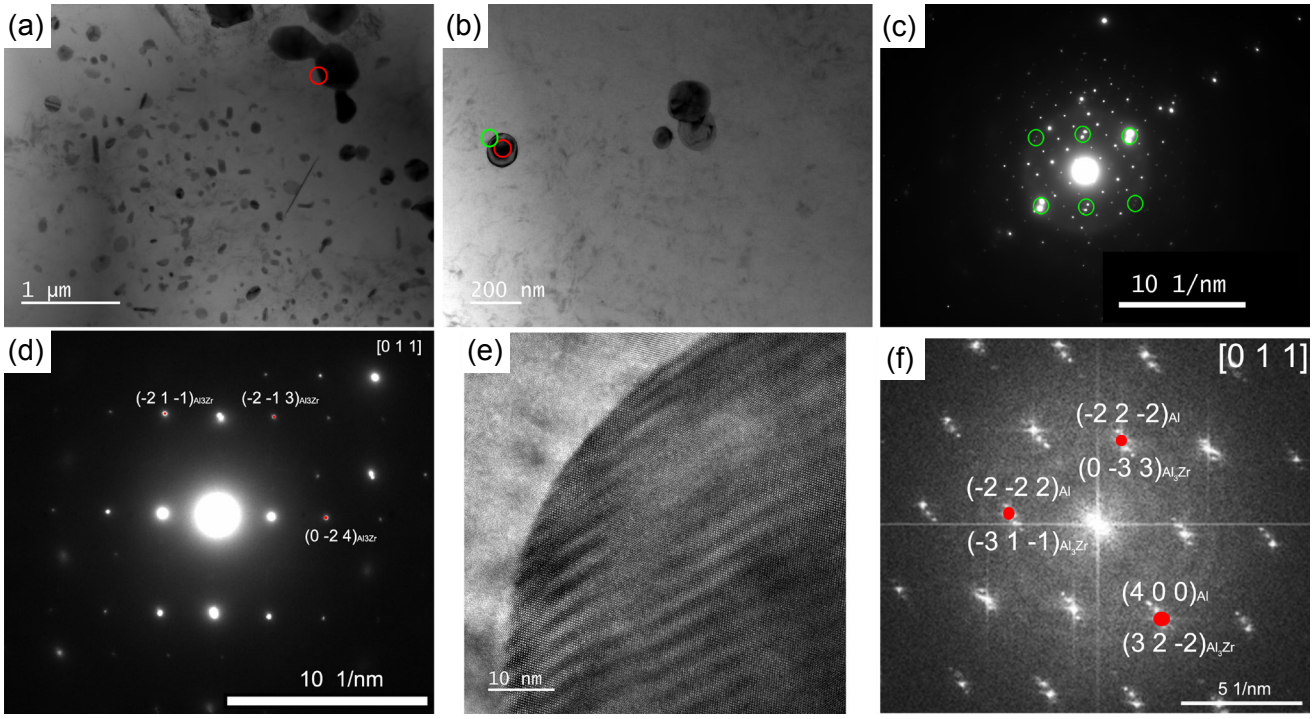

Fig. 8: TEM observations of intermetallic phase in Al-Si-Cu-Mg-(Zr-Mo) under T6 heat treatment condition: (a, b) microstructure; (c) diffraction spots in area selected by red circle in Fig. 8(a); (d) diffraction spots inside the red circle in Fig. 8(b); (e) photograph taken at high-resolution mode of the green area in Fig. 8(b); (f) diffraction spots obtained after fast Fourier transform in Fig. 8(e)

of Mo. In the study of Shu et al. [45], the addition of Mo has a significant effect on the nanoprecipitation phase, and the precipitation peak of the $L1_2$ nanoprecipitate phase is delayed by approximately 25 °C. Tang et al. [18] also noted that the addition of transition metal elements could participate in the formation of θ' phase. Due to the low diffusivity of transition metal elements, the anti-coarsening ability of the θ' phase is improved, and the strength and thermal stability of the intermediate phase are significantly improved. Comparing the DSC curve (Fig. 9) of Al-Si-Cu-Mg with that of Al-Si-Cu-Mg-(Zr-Mo), it is found that Al-Si-Cu-Mg shows two more peaks than Al-Si-Cu-Mg-(Zr-Mo). After combining the suggestions given in the references, the reactions corresponding to the three peaks were determined [46-48]. The reactions are shown in Table 4.

The disappearance of Peaks 1 and 2 means that Al_2Cu and Q-$Al_5Cu_2Mg_8Si_6$ phases are not synthesized in the

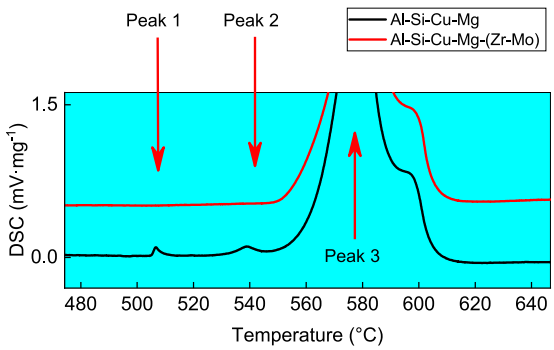

Fig. 9: DSC curves of Al-Si-Cu-Mg and Al-Si-Cu-Mg-(Zr-Mo)

Table 4: Phase reactions corresponding to three exothermic peaks in DSC curves

Peak	Reaction
Peak 1	Al_2Cu+Q-$Al_5Cu_2Mg_8Si_6$→Liquid
Peak 2	Q-$Al_5Cu_2Mg_8Si_6$+Si→Liquid
Peak 3	Si+other intermetallics→Liquid

Al-Si-Cu-Mg-(Zr-Mo) or other elements participate in the formation of these intermediate phases and raise the dissolution temperature. Of course, it is possible for both situations to occur simultaneously. As discussed in Section 3.1, for the larger-grain AlSiCuMo phase found by TEM observation, it is very likely that Mo participates in the synthesis of the Al-Al_2Cu-Si phase. This can not only hinder the precipitation of Al_2Cu and reduce the size of the Al_2Cu phase, but also improve the thermal stability of Al_2Cu. In addition, the Q-$Al_5Cu_2Mg_8Si_6$ phase is not found. Other Cu-containing intermetallic phases possibly have greater growth momentum when synthesizing other intermetallic phases. The Cu atoms originally used for the synthesis of the Q-$Al_5Cu_2Mg_8Si_6$ phase are used in advance, and thus the Q-$Al_5Cu_2Mg_8Si_6$ phase can not be synthesized [22]. Under the combined action of various factors mentioned above, Peaks 1 and 2 either disappear or are delayed until Peak 3, where eutectic silicon and intermetallic phases with transition metal elements dissolve. In any case, the alloy can withstand a higher solution temperature after the addition of Zr and Mo, which explains why the alloy has better heat resistance.

The sharp decrease in the mechanical properties of the alloy at high temperature is due to the coarsening and dissolution of the traditional intermetallic phases and the softening of the α-Al matrix. The alloy has greater free energy at higher temperatures, and the atoms obtain enough thermal activation energy to diffuse and cause more dislocation motion. With the increase in dislocation motion, many slip systems are activated. The grain boundary, as a region with high energy, produces relative motion between grains under the action of stress, so that the grain boundary loses the ability to hinder deformation. The intermetallic phase enriched with transition metal elements has good thermal stability and is well combined with the matrix, which can effectively hinder dislocation movement and crack propagation at this moment. This has also been confirmed in our previous study [32]. Figure 10 shows the dislocation behavior in the Al-Si-Cu-Mg-(Zr-Mo) alloy observed by TEM. The dislocation line is clearly blocked at the interface between the intermetallic phase and the matrix (white dotted line). These diffusion strengthening phases strengthen the alloy through the Friedel effect and Orawan mechanism [49]. When the dislocation movement approaches the edge of the strengthening phase, the small and not too hard precipitation phase is usually sheared by the movement of the dislocation (Friedel effect). When the precipitate is sufficiently large and strong, the mobile dislocations bypass the precipitate along the morphological appearance of the precipitate. The transition metal element-enriched strengthening phases formed in the Al-Si-Cu-Mg-(Zr-Mo) are dispersed in the alloy and are relatively hard, and maintain a good bonding state with the α-Al matrix at a temperature above 300 °C. This makes it possible to continue to effectively hinder the movement of dislocations after the failure of the traditional strengthening phase, thus play an extremely positive role in improving the mechanical properties at high temperatures. It also explains why those transition metal element-enriched strengthening phases have no significant effect on the improvement of the mechanical properties of the alloy at high temperature.

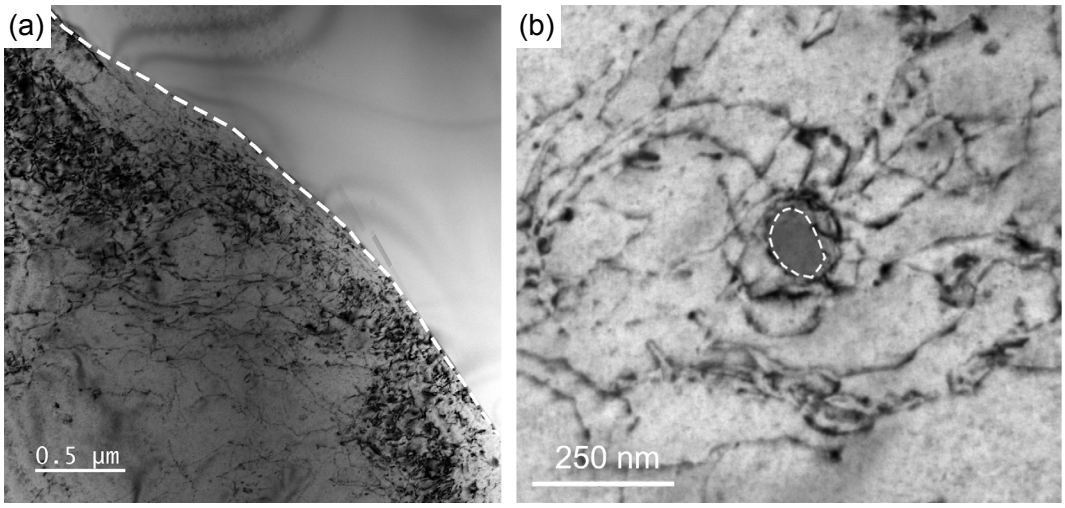

Fig. 10: TEM images of internal dislocation behavior in Al-Si-Cu-Mg-(Zr-Mo)

5 Conclusions

In this study, a modified Al-Si-Cu-Mg-(Zr-Mo) alloy was prepared by adding two transition metals, Zr and Mo, to an Al-Si-Cu-Mg base alloy, and the generated intermetallic phase was determined by combining results of EDS analysis and information from the literature. The metallographic structure and fracture structure were studied. The synergistic effect of Zr and Mo on the Al-Si-Cu-Mg alloy was quantitatively analyzed, and the strengthening mechanism was discussed. The main conclusions are as follows:

(1) The synergistic addition of Zr and Mo to the Al-Si-Cu-Mg base alloy generates a variety of Zr- and Mo-enriched intermetallic phases with good thermal stability, including nanoscale compounds and slightly larger microscale compounds.

(2) The nanodispersed Al_3Zr-type phase has good bonding with the α-Al matrix and can be used as a nucleation site to refine the grains. When the content of Si in the alloy is high, Si atoms partially replace Al atoms to form $(Al,Si)_3Zr$, and Ti atoms in the refiner also partially replace Zr atoms to form $(Al,Si)_3(TiZr)$. This increases the size of the nanodispersed phase from 20 nm to 80 nm.

(3) The addition of 0.2wt.% Zr and 0.2wt.% Mo improves the strength properties of the alloy, particularly when the test temperature is above 160 °C. At 300 °C, the UTS of the modified alloy is 85% greater than the peak value of the base alloy after T6 heat treatment.

(4) Intermetallic phases enriched with transition metal elements play a certain role in hindering dislocation movement and crack propagation, which improve the strength properties of the alloy by means of second-phase strengthening. In addition, the nanodispersed Al_3Zr-type phases improve the mechanical properties of the alloy through grain refinement strengthening.

(5) The participation of Mo in the formation of the traditional intermetallic phases inhibits their precipitation during aging, thereby reducing the size of the precipitates and improving their thermal stability.

(6) The newly formed intermetallic phases enriched with transition metal elements increase the solution temperature from 520 °C for the base alloy to 550 °C for the modified alloy, at which point the strengthening phases are fully diffused and uniform, and the peak mechanical properties are obtained. This can prove that the modified alloy has better heat resistance than the base alloy.

Acknowledgments

This work was supported by the Key R&D Program of Shandong Province of China (Grant number 2019QYTPY057), and the Natural Science Foundation of Shandong Province of China (Grant numbers ZR2020ME110, ZR2021ME023).

Conflict of interest

The authors declare that they have no conflicts of interest.

References

[1] Huter P, Oberfrank S, Grün F, et al. Thermo-mechanical fatigue influence of copper and silicon on hypo-eutectic Al-Si-Cu and Al-Si-Mg cast alloys used in cylinder heads. International Journal of Fatigue, 2016, 88: 142–155.

[2] Shaha S K, Czerwinski F, Kasprzak W, et al. Effect of Cr, Ti, V, and Zr micro-additions on microstructure and mechanical properties of the Al-Si-Cu-Mg cast alloy. Metallurgical and Materials Transactions A, 2016, 47(5): 2396–2409.

[3] Zuo L, Ye B, Feng J, et al. Effect of Q-$Al_5Cu_2Mg_8Si_6$ phase on mechanical properties of Al-Si-Cu-Mg alloy at elevated temperature. Materials Science and Engineering: A, 2017, 693: 26–32.

[4] An Z, Yang W, Zhan H, et al. On the strengthening effect of Al-Cr-Si dispersoid in an Al-Si-Mg-Cu casting alloy with Cr addition. Materials Characterization, 2020, 166: 110457.

[5] Kim K, Bobel A, Baik S I, et al. Enhanced coarsening resistance of Q-phase in aluminum alloys by the addition of slow diffusing solutes. Materials Science and Engineering: A, 2018, 735: 318–323.

[6] Senthil K M, Vanmathi M, Sakthivel G. SiC reinforcement in the synthesis and characterization of A356/Al_2O_3/SiC/Gr reinforced composite–paving a way for the next generation of aircraft applications. Silicon, 2020, 13(8): 2737–2744.

[7] Panthglin C, Boontein S, Kajornchaiyakul J, et al. Microstructure and impression creep characteristics of A356-SiC composites containing Zr. International Journal of Metalcasting, 2021, 16(2): 783–797.

[8] Rometsch P A, Schaffer G B, Taylor J A. Mass balance characterisation of Al-7Si-Mg alloy microstructures as a function of solution treatment time. International Journal of Cast Metals Research, 2016, 14(1): 59–69.

[9] Beroual S, Boumerzoug Z, Paillard P, et al. Effects of heat treatment and addition of small amounts of Cu and Mg on the microstructure and mechanical properties of Al-Si-Cu and Al-Si-Mg cast alloys. Journal of Alloys and Compounds, 2019, 784: 1026–1035.

[10] Shabestari S G. The effect of iron and manganese on the formation of intermetallic compounds in aluminum-silicon alloys. Materials Science and Engineering: A, 2004, 383(2): 289–298.

[11] Sadeghi I, Wells M A, Esmaeili S. Effect of particle shape and size distribution on the dissolution behavior of Al_2Cu particles during homogenization in aluminum casting alloy Al-Si-Cu-Mg. Journal of Materials Processing Technology, 2018, 251: 232–240.

[12] Garza-Elizondo G H, Samuel A M, Valtierra S, et al. Effect of transition metals on the tensile properties of 354 alloy: Role of precipitation hardening. International Journal of Metalcasting, 2016, 11(3): 413–427.

[13] Rakhmonov J, Timelli G, Bonollo F. The effect of transition elements on high-temperature mechanical properties of Al-Si foundry alloys – A review. Advanced Engineering Materials, 2016, 18(7): 1096–1105.

[14] Hernandez-Sandoval J, Garza-Elizondo G H, Samuel A M, et al. The ambient and high temperature deformation behavior of Al-Si-Cu-Mg alloy with minor Ti, Zr, Ni additions. Materials & Design, 2014, 58: 89–101.

[15] Mohamed A M A, Samuel F H, Kahtani S A. Microstructure, tensile properties and fracture behavior of high temperature Al-Si-Mg-Cu cast alloys. Materials Science and Engineering: A, 2013, 577: 64–72.

[16] Shaha S K, Czerwinski F, Kasprzak W, et al. Ageing characteristics and high-temperature tensile properties of Al-Si-Cu-Mg alloys with micro-additions of Cr, Ti, V and Zr. Materials Science and Engineering: A, 2016, 652: 353–364.

[17] Shaha S K, Czerwinski F, Kasprzak W, et al. Ageing characteristics and high-temperature tensile properties of Al-Si-Cu-Mg alloys with micro-additions of Mo and Mn. Materials Science and Engineering: A, 2017, 684: 726–736.

[18] Tang K, Du Q, Li Y. Modelling microstructure evolution during casting, homogenization and ageing heat treatment of Al-Mg-Si-Cu-Fe-Mn alloys. Calphad, 2018, 63: 164–184.

[19] Senkov O N, Shagiev M R, Senkova S V, et al. Precipitation of Al_3(Sc,Zr) particles in an Al-Zn-Mg-Cu-Sc-Zr alloy during conventional solution heat treatment and its effect on tensile properties. Acta Materialia, 2008, 56(15): 3723–3738.

[20] Chen Y C, Fine M E, Weertman J R. Microstructural evolution and mechanical properties of rapidly solidified Al-Zr-V alloys at high temperatures. Acta Metallurgica et Materialia, 1990, 38(5): 771–780.

[21] Knipling K E, Dunand D C, Seidman D N. Nucleation and precipitation strengthening in dilute Al-Ti and Al-Zr alloys. Metallurgical and Materials Transactions A, 2007, 38(10): 2552–2563.

[22] Zhang M, Liu K, Han J, et al. Investigating the role of Cu, Zr and V on the evolution of microstructure and properties of Al-Si-Mg cast alloys. Materials Today Communications, 2021, 26.

[23] de Luca A, Shu S, Seidman D N. Effect of microadditions of Mn and Mo on dual L12- and α-precipitation in a dilute Al-Zr-Sc-Er-Si alloy. Materials Characterization, 2020, 169.

[24] Dorin T, Babaniaris S, Jiang L, et al. Stability and stoichiometry of L12 Al_3(Sc,Zr) dispersoids in Al-(Si)-Sc-Zr alloys. Acta Materialia, 2021, 216.

[25] Rahimian M, Amirkhanlou S, Blake P, et al. Nanoscale Zr-containing precipitates; A solution for significant improvement of high-temperature strength in Al-Si-Cu-Mg alloys. Materials Science and Engineering: A, 2018, 721: 328–338.

[26] Sepehrband P, Mahmudi R, Khomamizadeh F. Effect of Zr addition on the aging behavior of A319 aluminum cast alloy. Scripta Materialia, 2005, 52(4): 253–257.

[27] Knipling K. Precipitation evolution in Al-Zr and Al-Zr-Ti alloys during aging at 450–600°C. Acta Materialia, 2008, 56(6): 1182–1195.

[28] Liu W, Xiao W, Xu C, et al. Synergistic effects of Gd and Zr on grain refinement and eutectic Si modification of Al-Si cast alloy. Materials Science and Engineering: A, 2017, 693: 93–100.
[29] Morri A, Ceschini L, Messieri S, et al. Mo addition to the A354 (Al-Si-Cu-Mg) casting alloy: Effects on microstructure and mechanical properties at room and high temperature. Metals, 2018, 8(6): 393.
[30] Farkoosh A R, Grant Chen X, Pekguleryuz M. Dispersoid strengthening of a high temperature Al-Si-Cu-Mg alloy via Mo addition. Materials Science and Engineering: A, 2015, 620: 181–189.
[31] Zamani M, Seifeddine S, Jarfors A E W. High temperature tensile deformation behavior and failure mechanismsof an Al-Si-Cu-Mg cast alloy – The microstructural scale effect. Materials and Design, 2015: 10.
[32] Gao C, Zhang L K, Zhang B R. Effect of transition metal elements on high-temperature properties of Al-Si-Cu-Mg alloys. Metals, 2021, 11(2): 357.
[33] Gao T, Zhu X, Sun Q, et al. Morphological evolution of ZrAlSi phase and its impact on the elevated-temperature properties of Al-Si piston alloy. Journal of Alloys and Compounds, 2013, 567: 82–88.
[34] Ceschini L, Morri A, Toschi S, et al. Microstructural and mechanical properties characterization of heat treated and overaged cast A354 alloy with various SDAS at room and elevated temperature. Materials Science and Engineering: A, 2015, 648: 340–349.
[35] Liu S, Zhang X, Peng H L, et al. In situ nanocrystals manipulate solidification behavior and microstructures of hypereutectic Al-Si alloys by Zr-based amorphous alloys. Journal of Materials Research and Technology, 2020, 9(3): 4644–4654.
[36] Knipling K E, Karnesky R A, Lee C P, et al. Precipitation evolution in Al-0.1Sc, Al-0.1Zr and Al-0.1Sc-0.1Zr (at.%) alloys during isochronal aging. Acta Materialia, 2010, 58(15): 5184–5195.
[37] Mao G L, Tong G Z, Gao W L, et al. The poisoning effect of Sc or Zr in grain refinement of Al-Si-Mg alloy with Al-Ti-B. Materials Letters, 2021, 302: 130428.
[38] Mahmudi R, Sepehrband P, Ghasemi H M. Improved properties of A319 aluminum casting alloy modified with Zr. Materials Letters, 2006, 60(21–22): 2606–2610.
[39] Gao T, Ceguerra A, Breen A, et al. Precipitation behaviors of cubic and tetragonal Zr-rich phase in Al-(Si-)Zr alloys. Journal of Alloys and Compounds, 2016, 674: 125–130.
[40] Knipling K, Dunand D. Creep resistance of cast and aged Al-0.1Zr and Al-0.1Zr-0.1Ti (at.%) alloys at 300–400°C. Scripta Materialia, 2008, 59(4): 387–390.
[41] Zhang Z, Du X, Zhuang P, et al. Microstructure and mechanical properties of Zr-modified Al-7Si-0.35Mg-0.2Ti cast alloy. Micro & Nano Letters, 2020, 15(10): 688–692.
[42] Wang F, Qiu D, Liu Z L, et al. The grain refinement mechanism of cast aluminium by zirconium. Acta Materialia, 2013, 61(15): 5636–5645.
[43] Farkoosh A R, Pekguleryuz M. Enhanced mechanical properties of an Al-Si-Cu-Mg alloy at 300 °C: Effects of Mg and the Q-precipitate phase. Materials Science and Engineering: A, 2015, 621: 277–286.
[44] Shower P, Roy S, Hawkins C S, et al. The effects of microstructural stability on the compressive response of two cast aluminum alloys up to 300 °C. Materials Science and Engineering: A, 2017, 700: 519–529.
[45] Shu S P, de Luca A, Dunand D C, et al. Individual and synergistic effects of Mn and Mo micro-additions on precipitation and strengthening of a dilute Al-Zr-Sc-Er-Si alloy. Materials Science and Engineering: A, 2021, 800: 140288.
[46] Yang Y, Zhong S Y, Chen Z, et al. Effect of Cr content and heat-treatment on the high temperature strength of eutectic Al-Si alloys. Journal of Alloys and Compounds, 2015, 647: 63–69.
[47] Zheng Y, Xiao W, Ge S, et al. Effects of Cu content and Cu/Mg ratio on the microstructure and mechanical properties of Al-Si-Cu-Mg alloys. Journal of Alloys and Compounds, 2015, 649: 291–296.
[48] Zamani M, Morini L, Ceschini L, et al. The role of transition metal additions on the ambient and elevated temperature properties of Al-Si alloys. Materials Science and Engineering: A, 2017, 693: 42–50.
[49] Sjölande R E, Seifeddine S. The heat treatment of Al-Si-Cu-Mg casting alloys. Journal of Materials Processing Technology, 2010, 210(10): 1249–1259.